SAND REPORT
SAND2003-4620
Unlimited Release
Printed December 2003

Investigation of 2D Laterally Dispersive Photonic Crystal Structures LDRD 33602 Final Report

David W. Peters, Joel R. Wendt, G. Ronald Hadley, G. Allen Vawter, Greg Peake, Junpeng Guo. Ganesh Subramania

Prepared by
Sandia National Laboratories
Albuquerque, New Mexico 87185 and Livermore, California 94550

Sandia is a multiprogram laboratory operated by Sandia Corporation, a Lockheed Martin Company, for the United States Department of Energy's National Nuclear Security Administration under Contract DE-AC04-94-AL85000.

Approved for public release; further dissemination unlimited.

Sandia National Laboratories

Issued by Sandia National Laboratories, operated for the United States Department of Energy by Sandia Corporation.

NOTICE: This report was prepared as an account of work sponsored by an agency of the United States Government. Neither the United States Government, nor any agency thereof, nor any of their employees, nor any of their contractors, subcontractors, or their employees, make any warranty, express or implied, or assume any legal liability or responsibility for the accuracy, completeness, or usefulness of any information, apparatus, product, or process disclosed, or represent that its use would not infringe privately owned rights. Reference herein to any specific commercial product, process, or service by trade name, trademark, manufacturer, or otherwise, does not necessarily constitute or imply its endorsement, recommendation, or favoring by the United States Government, any agency thereof, or any of their contractors or subcontractors. The views and opinions expressed herein do not necessarily state or reflect those of the United States Government, any agency thereof, or any of their contractors.

Printed in the United States of America. This report has been reproduced directly from the best available copy.

Available to DOE and DOE contractors from
U.S. Department of Energy
Office of Scientific and Technical Information
P.O. Box 62
Oak Ridge, TN 37831

Telephone: (865)576-8401
Facsimile: (865)576-5728
E-Mail: reports@adonis.osti.gov
Online ordering: http://www.doe.gov/bridge

Available to the public from
U.S. Department of Commerce
National Technical Information Service
5285 Port Royal Rd
Springfield, VA 22161

Telephone: (800)553-6847
Facsimile: (703)605-6900
E-Mail: orders@ntis.fedworld.gov
Online order: http://www.ntis.gov/help/ordermethods.asp?loc=7-4-0#online

SAND2003-4620
Unlimited Release
Printed December 2003

Investigation of 2D Laterally Dispersive Photonic Crystal Structures LDRD 33602 Final Report

David W. Peters and Joel R. Wendt
Photonic Microsystems Technology

G. Ronald Hadley, G. Allen Vawter, Greg Peake and Junpeng Guo
RF Microsystems Technologies

Ganesh Subramania
Photonic Microsystems Technology

Sandia National Laboratories
PO Box 5800
Albuquerque, NM 87185-0603

Abstract

Artificially structured photonic lattice materials are commonly investigated for their unique ability to block and guide light. However, an exciting aspect of photonic lattices which has received relatively little attention is the extremely high refractive index dispersion within the range of frequencies capable of propagating within the photonic lattice material. In fact, it has been proposed that a negative refractive index may be realized with the correct photonic lattice configuration. This report summarizes our investigation, both numerically and experimentally, into the design and performance of such photonic lattice materials intended to optimize the dispersion of refractive index in order to realize new classes of photonic devices.

Extensive simulation and design of laterally dispersive photonic lattice lens is presented, including design of a unique structure to improve coupling of light into row-defect photonic lattice waveguides. Optical losses are identified as a key factor limiting the utility of such dispersive elements. Results of a groundbreaking theoretical investigation of optical loss in transmission through a photonic lattice waveguide are presented. Finally, our experimental investigation into the fabrication and testing of a laterally dispersive photonic lens is presented. Final conclusions suggest that losses in transmission through laterally dispersive photonic lattice devices designed to operate above the light line prohibit any useful application of these devices at this time. Further technology development, at Sandia and elsewhere, is needed to reduce optical losses.

Table of Contents

Introduction

Three-dimensional photonic crystals (PCs) offer ways of controlling light not found in other structures. Two-dimensional PCs do not offer the same degree of control over light propagation, however the fabrication processes and possibilities for integration with other elements make devices made from two-dimensional PCs worth investigating. PCs offer mechanisms not commonly seen in other optical materials; these mechanisms can be exploited to develop photonic devices not possible with traditional optical materials. Development of structures using these mechanisms unique to PCs is essential for PC integration into applications. Here we apply one such mechanism to mitigate a problem seen in coupling light in PC waveguides.

One PC structure integral to many possible devices is the row-defect waveguide, where removal of one or more rows of holes in the PC creates a path for light to propagate. Unlike traditional waveguides, PC waveguides allow sharp bends to be made. Innovative splitters and WDM devices have been proposed using row-defect waveguides. Here we focus on waveguides where a single row of holes has been eliminated. These single-row defect waveguides have been extensively studied, both numerically and experimentally.

We explore a fundamental and crucial aspect of these structures: coupling light into a row-defect waveguide from a uniform bulk material. A drawback to single-row defect waveguides is that efficient coupling from the bulk material into row-defect waveguides in photonic crystals has proven difficult. Methods of improving the coupling have been explored, including the introduction of defects and/or the tapering of the photonic crystal at the entrance to the row-defect waveguide. A more elaborate reflective structure has also been designed and fabricated that reflects and focuses light from a traditional waveguide into a PC waveguide [1].

We describe an alternate method for increasing the coupling taking advantage of the highly dispersive nature of photonic crystals at particular wavelengths. Research has shown that photonic crystals can exhibit a negative refractive index when particular modes are excited over a certain range of angles [2]. We will show that this phenomenon can be used to substantially increase the coupled power into a row-defect waveguide. By utilizing the negative-refraction behavior demonstrated by some photonic crystal modes, this coupling can be greatly enhanced by using the focusing effect that such a negative index can offer.

Three-dimensional modeling of the row-defect waveguide shows out-of-plane loss into the substrate and cover regions. This extremely difficult computational effort illustrates a significant advancement in Sandia's numerical modeling capabilities generated by work on these complex photonic crystals. Losses are found to be significant in some wavelength ranges, as has been observed experimentally.

Negative Refraction

The negative refractive index observed when some photonic crystal modes are excited causes a beam of light to bend in the "wrong" direction, an impossibility in ordinary materials. This effect is a recent development in the optical frequencies, described theoretically by Notomi in 2000 [2], and observed experimentally by Kosaka, u sing 3D template-type photonic crystals, in 1998. [3] A material with a negative index of refraction is of great interest and has utility beyond the backward bending of a beam of light. Such materials offer the ability of lensing and guiding light in ways not possible with ordinary materials.

Negative refraction does not occur for all frequencies of light entering a photonic crystal. As in multimode waveguides, light propagation in photonic crystals occurs in discrete modes. Each of these modes has independent dispersion characteristics. Some modes exhibit characteristics that closely resemble those of light propagating in ordinary materials. No unusual behavior is therefore observed in these modes. However, certain modes of photonic crystals exhibit anomalous behavior. This behavior can be explained with an equifrequency diagram for the given photonic crystal mode.

The propagation of light is often represented in momentum space where frequency, ω, is plotted as a function of the wave vector, k. In bulk isotropic materials $k=c/n\lambda$. Equifrequency contours for a uniform bulk material are circles (spheres if all three dimensions of propagation are considered). The radii of these circles increase with increasing frequency. The direction of light propagation in a material is determined by the gradient, $d\omega/dk$. For these circular shapes of increasing size (k increases as ω increases), this direction will always point outward and leads to the familiar behavior we expect for light propagation and for the bending of light at interfaces between two such materials. This behavior is illustrated in *Fig. 1* as light travels from the top medium to the lower medium.

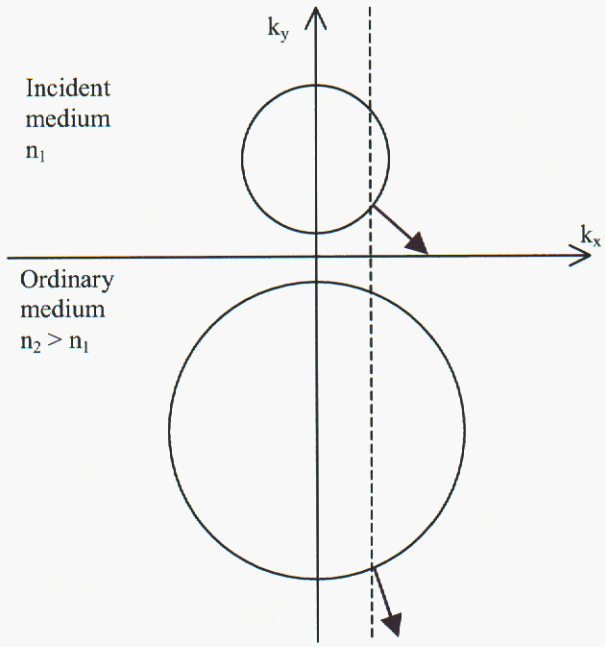

Fig. 1. Propagation of light across a boundary of two ordinary materials

In photonic crystals, this behavior is seen in some modes of propagation. However, other modes exist in photonic crystals that exhibit two forms of anomalous behavior that deviate from the simple case of bulk material. Each of these anomalies, if found independently, will lead to negative refraction. However, if they were both present, the effects would lead to positive refraction. The first of these effects occurs when the equifrequency surface has increasing radii with increasing frequency, but has a section that exhibits a concave surface. In this case, the gradient now points inward rather than outward. This situation is seen in the colored equifrequency curves of *Fig. 2a*. Only one-sixth of the equifrequency contours are shown for the photonic crystal, symmetry may be used to complete the entire contour. The second effect is seen when a mode has equifrequency surfaces that decrease in radii with increasing frequency over a frequency range. Again, the gradient is now opposite from the case of a bulk material as seen in *Fig. 2b*. Data for these two figures are from code developed for this project, and represent actual modes of a hexagonal two-dimensional photonic crystal.

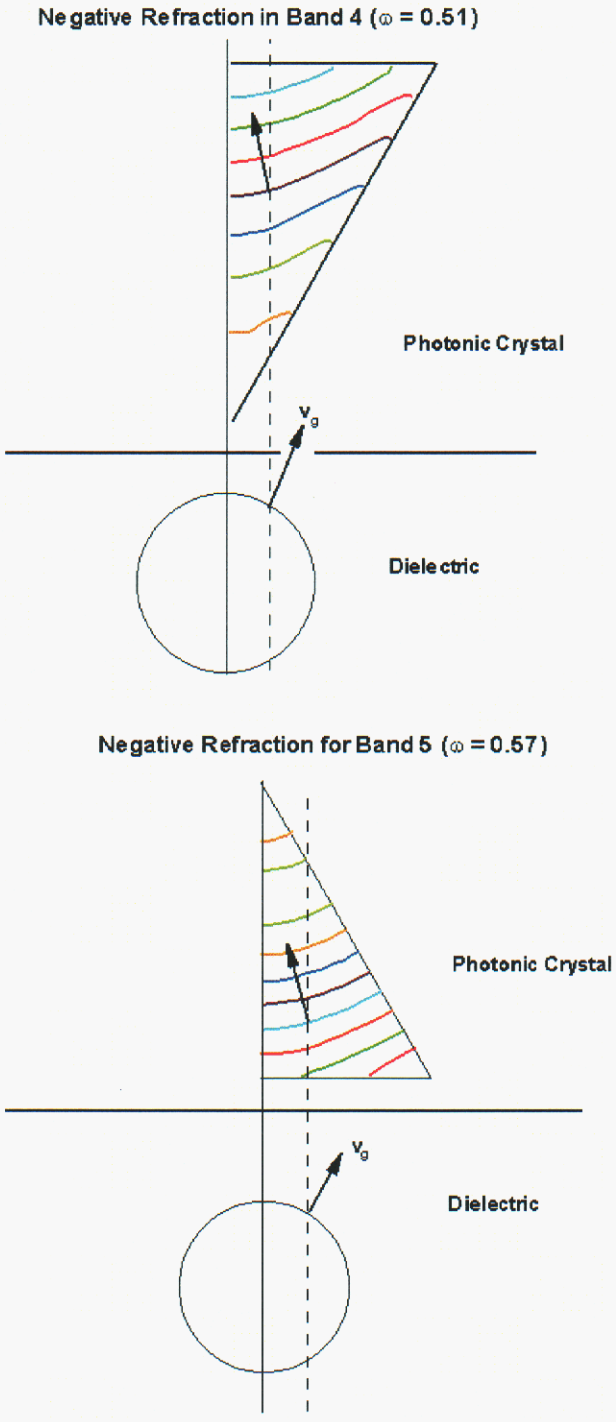

Fig. 2. Two cases for propagation of light across a boundary of an ordinary material and a photonic crystal exhibiting anomalous equifrequency surfaces

This behavior can occur over a range of incident angles and wavelengths. A diverging Gaussian beam may therefore converge to a small spot, which may then be used for coupling into a single-row defect waveguide of a second photonic crystal.

For this LDRD we studied a photonic crystal with a mode exhibiting the behavior shown in *Fig. 2a*. The photonic crystal is fabricated on a GaAs wafer that has a high-aluminum-content layer, that when oxidized produces a low-index cladding layer. A high-index waveguiding layer of GaAs acts as the waveguiding layer, while the upper cladding is a thin layer of SiO2. A photonic crystal in a triangular pattern is then etched through the cladding and waveguide layers into the substrate. The basic design is shown in *Fig. 3*. Fabrication details for this structure will be detailed later in this report.

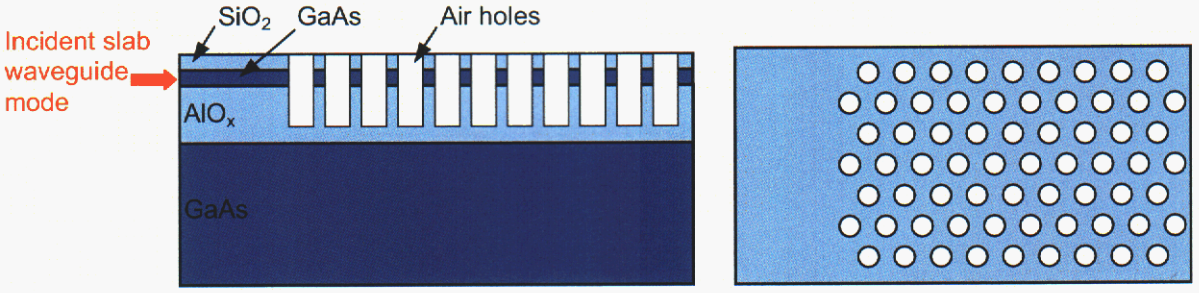

Fig. 3. Photonic crystal structure

The negative refraction is observable numerically over a range of angles. Light entering into a photonic crystal exhibiting negative refraction can be seen in *Fig. 4* and in *Fig. 5* at 3° and 8°, respectively. The numerical modeling method used to obtain these results will be discussed in the 2D modeling section later in this report. Some reflectivity from the upper boundary can be seen in the 3° plot. *Fig. 5* also demonstrates a secondary effect discovered in performing these calculations. Note that the beam neither converges nor diverges as it propagates through the photonic crystal. This surprising collimation effect merits additional discussion and will be explored further in a later section.

The support of this negative refraction over a range of angles allows the focusing of a diverging beam. The reason for this wide region can be again drawn from the equifrequency diagram. The relative closeness of the contours to a circular shape ensures a smooth transition of output angle as a function of input angle. A Gaussian beam with a range of angular frequency will be transformed into a Gaussian with a corresponding range of angular frequencies inside the photonic crystal, but with the angles reversed. Thus a diverging beam will be converted to a converging beam. A diverging Gaussian is incident on a bulk material/PC interface in *Fig. 6,* the interface being at the bottom of the simulated region. The focusing of this beam to a small area is clear.

The equifrequency surfaces for the mode of the photonic crystal that produced these effects are shown in *Fig. 7.* Note the decreasing radii of the equifrequency contours with increasing frequency in this frequency range as in the second example of *Fig. 2.*

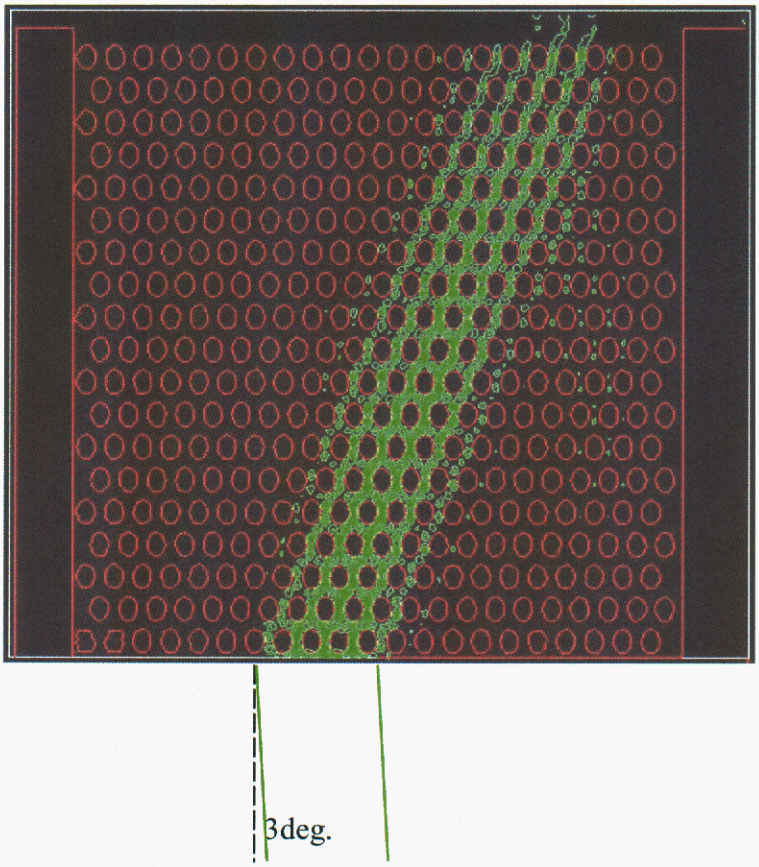

Fig. 4. Photonic crystal with input Gaussian beam incident at 3° from normal exhibiting negative refraction

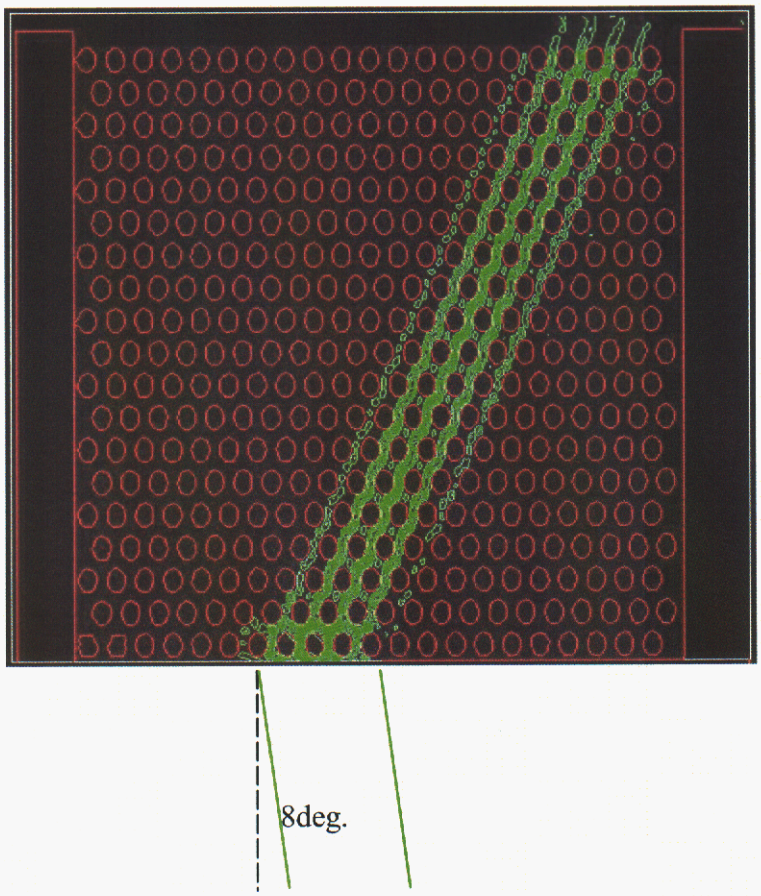

Fig. 5. Photonic crystal with input Gaussian beam incident at 8° from normal exhibiting negative refraction

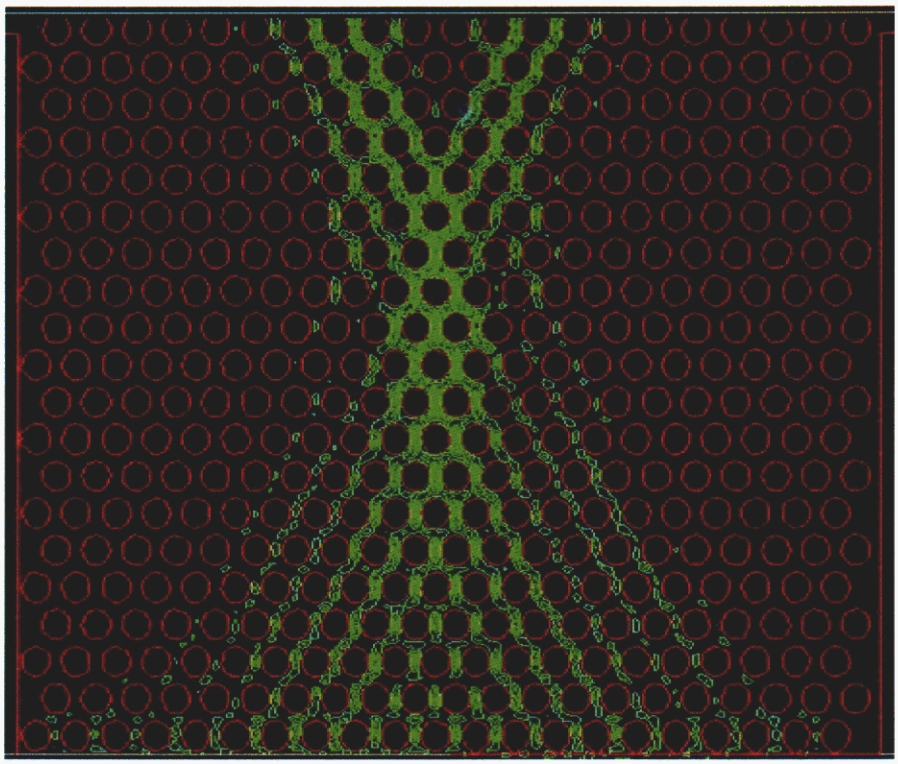

Fig. 6. Focusing of a diverging Gaussian using the negative refraction behavior of a hexagonal photonic crystal

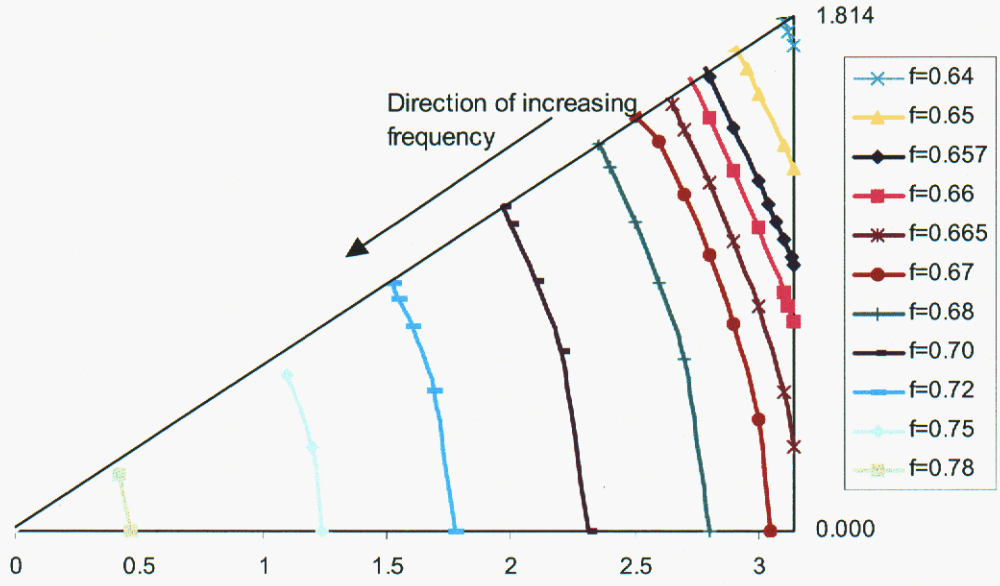

Fig. 7. Equifrequency plot for 2D PC showing decreasing radii with increasing frequency

Direct Coupling

Before introducing the focusing PC into the coupling issue, we should first discuss the direct coupling of a beam of light from a bulk material into a PC row-defect waveguide. Direct coupling into a single-row defect waveguide is difficult because of the small size of the waveguiding channel, less than a single freespace wavelength in width. Efficient coupling requires a beam of extraordinarily small size. To model the coupling, we used the same two-dimensional code as for the negative refraction examples of the previous section.

The incident mode seen in *Fig. 8* is a Gaussian inside the bulk effective index material. The coupling efficiency is determined by comparing the total power of the input Gaussian beam to the power in the row-defect waveguide at the opposite end of the simulation region. The Gaussian beam was varied in width to determine its effect on coupling efficiency.

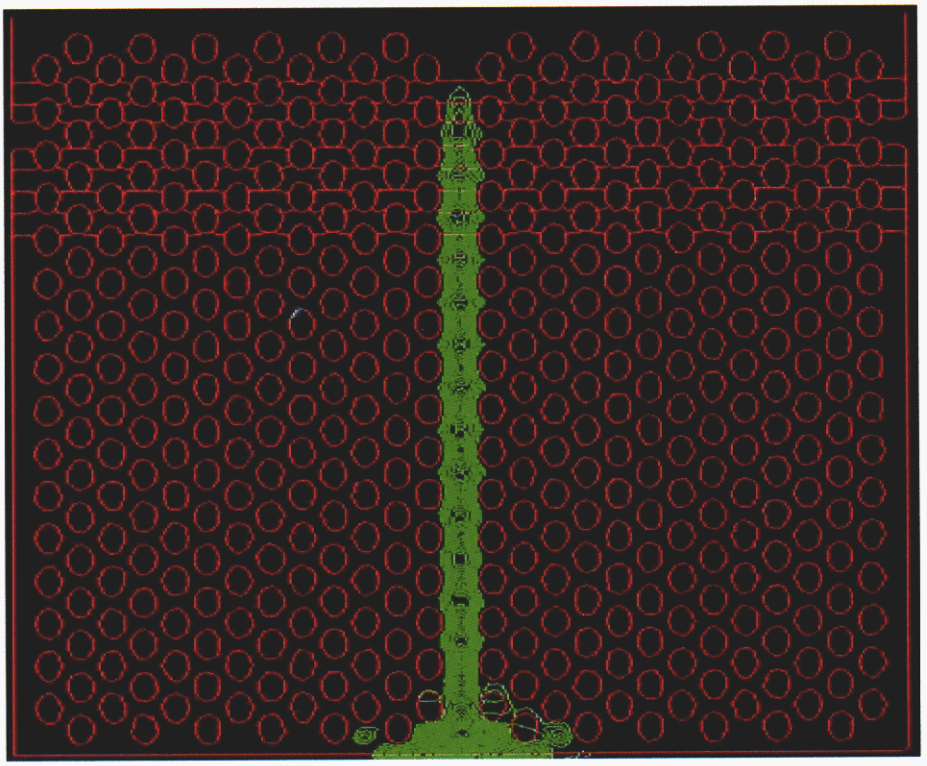

Fig. 8. Direct coupling into a single-row-defect photonic crystal waveguide using a narrow Gaussian beam

As the dimension of a Gaussian beam is increased, the coupling efficiency quickly drops as seen in *Fig. 9.* For efficient coupling, the Gaussian beam needs to have a width that is on the order of the free-space wavelength; obviously, this is not practical. Moreover, to obtain the higher efficiencies seen on this plot there must also be sub-wavelength

precision in the lateral placement of the beam. This sensitivity to beam location can be alleviated by using a wider input beam, however peak efficiency is then guaranteed to be a lower value as seen in *Fig. 10.* Direct coupling of a Gaussian beam into a single-row defect waveguide is therefore inherently inefficient for all practical situations.

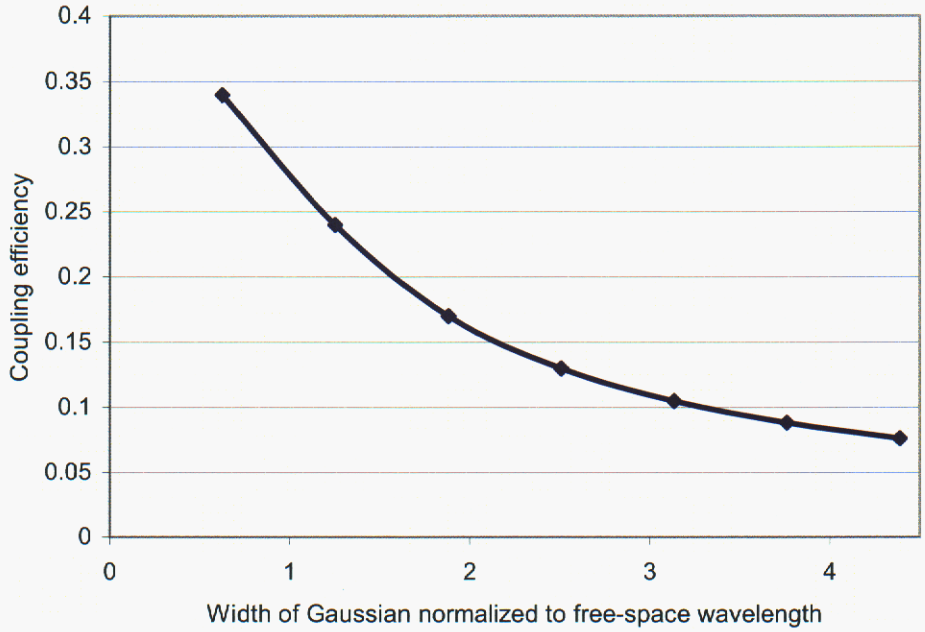

Fig. 9. Efficiency of direct coupling into a single-row defect waveguide

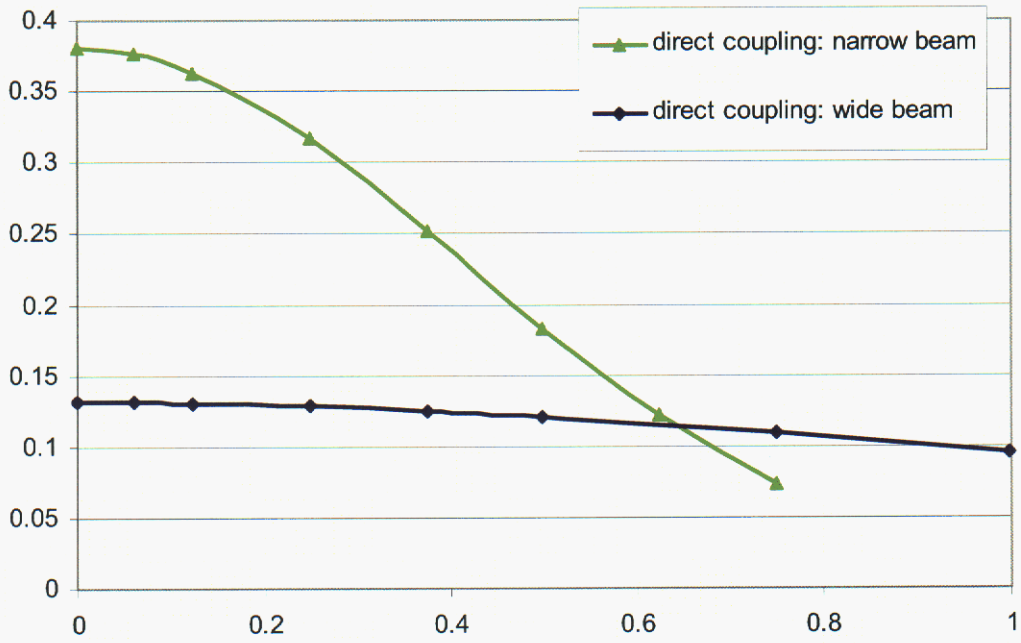

Fig. 10. Coupling efficiency as a function of lateral offset of the input Gaussian beam

Coupling

To obtain both the focusing behavior and the row-defect waveguide, two variants of the same photonic crystal are used on the same substrate. A 90-degree rotation is required, as is a change in lattice constant. Combining these two different lattice designs creates a photonic crystal heterostructure. Using a Helmholtz code to model the 2D photonic crystal structures, we show that by using this geometry, a five-fold increase in efficiency is obtained over direct coupling.

Creating the focusing effect requires use of a frequency band above the light line. The light line is the boundary in frequency space above which radiation of light out of the photonic crystal is permitted and out-of-plane losses are high. For efficient transmission the losses in this band are prohibitive however. Therefore, for the row-defect waveguide a band operating below the light-line is preferable. As the wavelength is obviously a constant, the lattice constant in these two sections must differ. A rotation by 90 degrees of the two lattices is also required; the resulting structure with the inserted focusing photonic crystal region appears in *Fig. 11.* As the photonic crystal structures are defined by e-beam lithography, the relative distance and lateral alignment between the two photonic crystal regions may be carefully controlled.

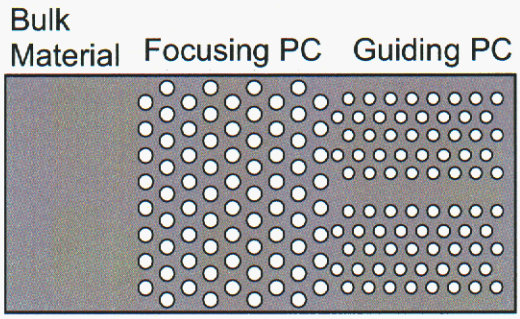

Fig. 11. Alignment of focusing and waveguiding photonic crystals

Results of this computation are shown in *Fig. 12.* The focusing of light to a small region in the vicinity of the entrance to the row-defect waveguide can be seen. Lines at the top of the simulation space are absorbing regions of increasing strength, used to minimize reflections from the top boundary.

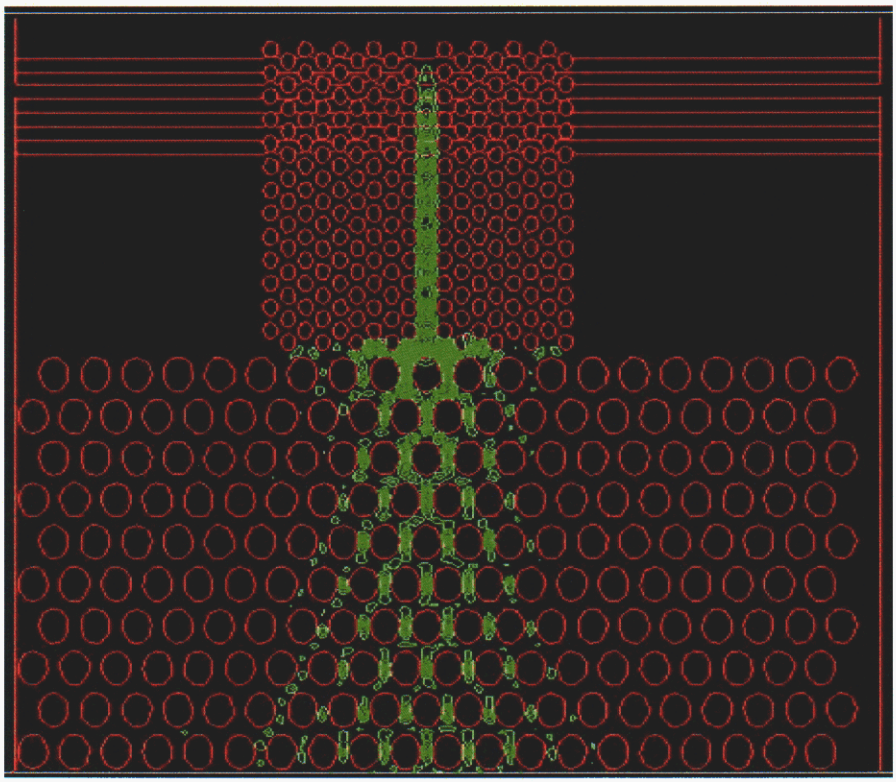

Fig. 12. Coupling into a single-row-defect waveguide using a photonic crystal operating in a negative refraction regime

One of the desired benefits of such a coupling system would be the decrease in tolerances required for efficient coupling to occur. Variations that can be foreseen include

differences in the focal length of the diverging beam and lateral offset of this beam. Both of these possible deleterious effects were investigated. In *Fig. 13* the effect of frequency variation is seen, a broad region of efficient coupling is found in the region of a_1/λ of 0.66, with a second peak occurring at higher frequency. The effect of the degree of divergence of the incoming Gaussian beam is even less sensitive to variation as seen in *Fig. 14*. Greater than 40% coupling can be achieved with the focal length changing by a factor of three. For these calculations the length of the focusing photonic crystal remained constant, with the input beam focal length allowed to vary.

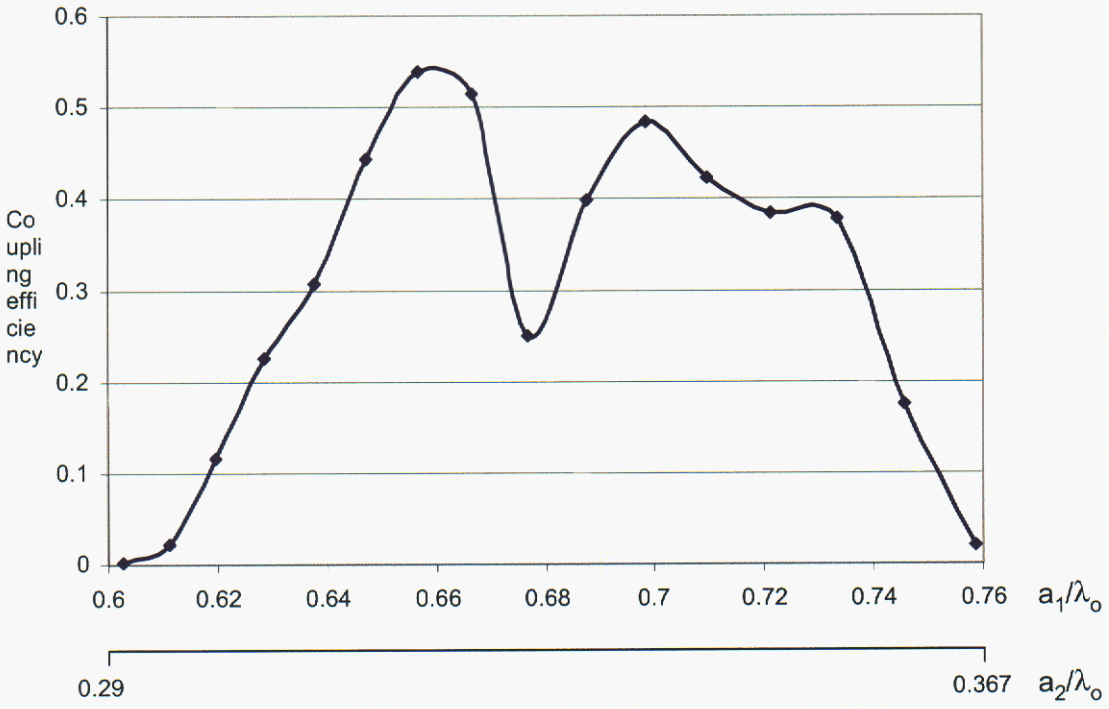

Fig. 13. Coupling efficiency as a function of frequency

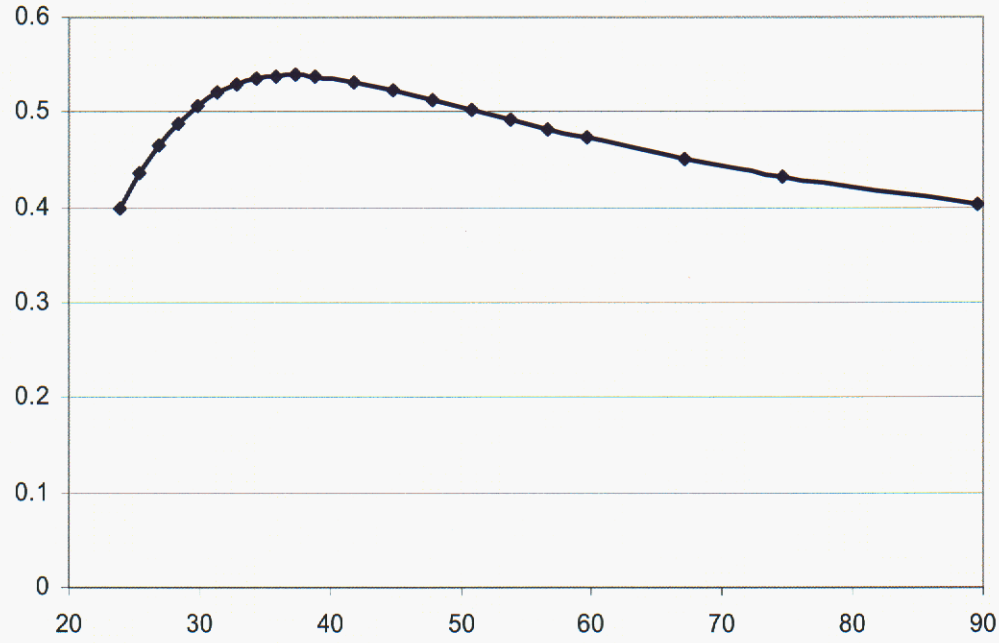

Fig. 14. Coupling efficiency as a function of focal length of beam in bulk region

Self-Collimation of Light Propagating in Photonic Crystals

Our calculations are some of the first numerical results showing self-collimation of light propagating in photonic crystals without any laterally patterned waveguide feature. The consequences of this effect could be substantial. This represents a waveguiding method for light without a waveguiding channel. Beams may thus cross without any interference or loss at the intersection. The equifrequency diagram also explains this behavior. In this case, a section of the equifrequency surface that is relatively flat is used. As seen in *Fig. 15,* there is a range of angles in the incident medium that results in a collimated beam in the photonic crystal. These "preferred directions" inside the photonic crystal have been observed in both the hexagonal array and the square array of holes. The example shown in *Fig. 15* is for a square lattice of holes. A strongly diverging Gaussian beam is used as the input at the lower boundary, yet no divergence is seen in the photonic crystal. Unlike the photonic crystal used in the focusing section of the earlier device, this effect is seen in a much lower-loss region of the band diagram. Future exploration of this area is warranted, as the losses associated with row-defect waveguides could be avoided by using such a waveguiding scheme.

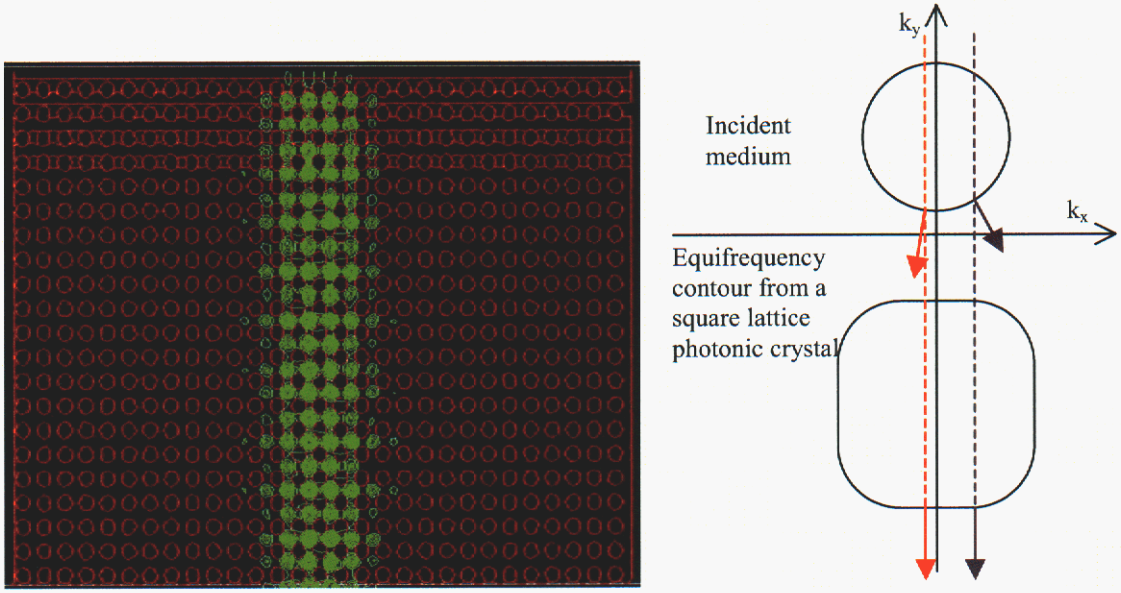

Fig. 15. Simulation result and qualitative equifrequency contour of a photonic crystal with a square lattice that collimates light and offers "waveguideless waveguiding". The frequency of the light used in the self-collimating simulations is below the light line, thus low-loss is to be expected. The lattice constant-to-wavelength ratio, a/l is in the region of 0.32, although the behavior is observable in a range about this value.

An additional aspect of the collimating behavior that we have been unable to explain theoretically to date is a "phase-freezing" effect. It appears that a phase front can be held across a propagating distance in the collimating photonic crystal while maintaining a phase front that is actually diverging. In *Fig. 16* we see a diverging Gaussian propagate through a square lattice where it is collimated. However, upon reaching the second photonic crystal it converges in a manner similar to earlier examples without the presence of the square lattice photonic crystal.

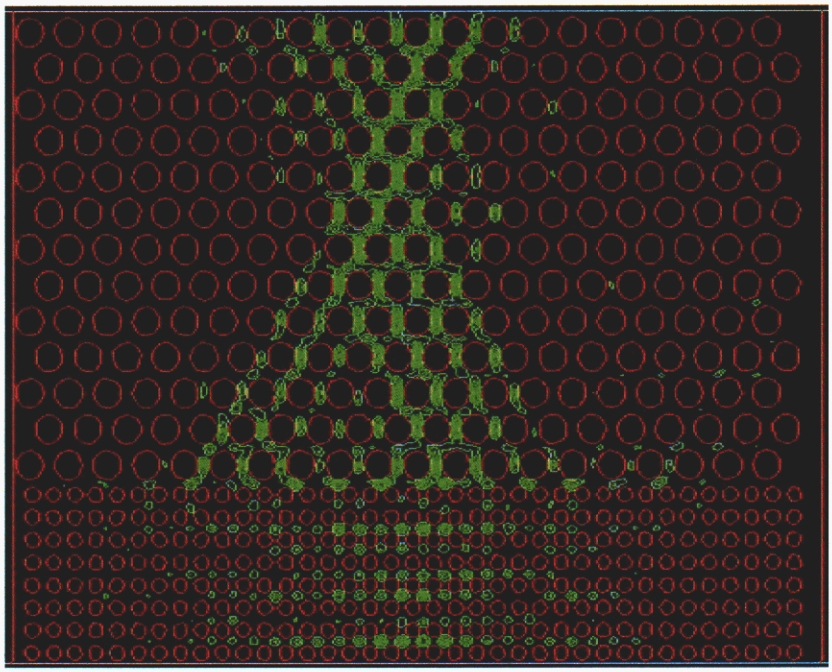

Fig. 16. "Phase-freezing" of diverging Gaussian across a square lattice photonic crystal

2D Modeling

Three-dimensional modeling is extremely slow and computer intensive. Computer resources available to us did not allow for three-dimensional modeling of the entire structure. Appropriate simplifications of the three-dimensional structure can allow modeling in two dimensions. This simplification allows the modeling of a photonic crystal structure comprised of a focusing section and a row defect waveguide. A typical run of a single wavelength would take approximately two minutes.

The program used is a semi-vectorial Helmholtz equation code. A triangular mesh is employed to avoid the stair stepping errors that occur at curved boundaries (such as the holes of a photonic crystal) if a square mesh is used. Absorbing boundary conditions were used at the entrance face to absorb reflections from the front surface of the photonic crystal. Absorbing boundaries were also used at the two side surfaces of the simulated region. At the boundary opposite the side where light is incident both a radiation boundary condition and a radiation boundary condition with an absorber in front of it were tried. A graded absorbing boundary where the imaginary component of the refractive index is increased in steps as the radiation boundary is approached yielded good results in most cases.

The refractive index of the bulk material into which the photonic crystal holes are etched varies with depth in the actual structure. In a two-dimensional model this is not possible as no variation is allowed in the third dimension. To account for this limitation, the

modal index of the guided mode in the slab waveguide is used for the bulk index in the photonic crystal. For the thicknesses used, and for the wavelength range of interest, this effective index came out to be around 3.01. This value was then used as the refractive index for the bulk material for all simulations. The two-dimensional problem now appears as the top view of *Fig. 3b,* with no variation in depth.

Unfortunately, two-dimensional modeling cannot predict losses out of the plane of the waveguide as this dimension is assumed infinite and non-varying in extent. Some two-dimensional photonic crystals have exhibited extremely high out-of-plane losses, making this component of photonic crystal design an important area of research. For this aspect of photonic crystal design a fully three-dimensional code was required.

3D Modeling and Intrinsic Loss of 2D Photonic Crystals

Although many effects of interest, including negative refraction, can be studied using 2D models together with the effective index method, the issue of propagation loss in photonic crystal structures is inherently a 3D problem and can therefore only be studied using 3D modeling. While it is true that roughness scattering or fabrication imperfections can also lead to loss (and could be studied in 2D), these losses are generally small compared to out-of-plane losses and are non-intrinsic; i.e. they can be decreased to arbitrarily small levels by improvements in fabrication. In contrast, out-of-plane losses are intrinsic to the photonic crystal structure and must be thoroughly understood if low-loss circuits are to be designed.

Our study of out-of-plane losses was deliberately narrowed to center on losses in single-row-defect waveguides, since it was expected that the wave in such structures would be laterally confined, and thus the 3D modeling could be affected using a smaller problem region. The calculations are thus specific to this waveguide structure, although the same basic mechanisms are expected to be operative in unperturbed regions as well.

Single-row-defect waveguides are produced by altering or removing the holes in a single row along the Γ-X direction, thus forming an altered channel that will confine light. We initially modeled these waveguides in 2D, resulting in the undulating modes shown in *Fig. 17.* A triangular mesh was employed in order to resolve the circles as accurately as possible and avoid stair-stepping errors that can become prominent whenever curved interfaces between high-index-contrast materials are modeled using a rectangular grid. 3D modeling was then attempted by considering only a unit cell in the propagation direction, as outlined by the dashed line, keeping as many rows of holes in the lateral direction as necessary, and adding a depth grid of uniform zones. A finite difference analogue of the 3D Helmholtz Equation was derived and solved numerically on the resulting grid as an eigenproblem whose eigenvalue was the complex propagation constant. Out-of-plane radiation was collected at the top and bottom boundaries either by using absorbing materials or, later on, by a semi-analytic mode expansion radiation

boundary condition. The latter was introduced after initial 1D slab radiation mode calculations made using absorbing layers were found to lead to spurious radiation modes that were not present when the exact radiation boundary condition was used. Of course, in the full 3D simulations the mode-expansion radiation boundary condition is only exact when all possible modes are included, and so for finite problem size must be considered approximate. This uncertainty in treating the radiation loss was unexpected and became one of two major problems encountered with this calculation.

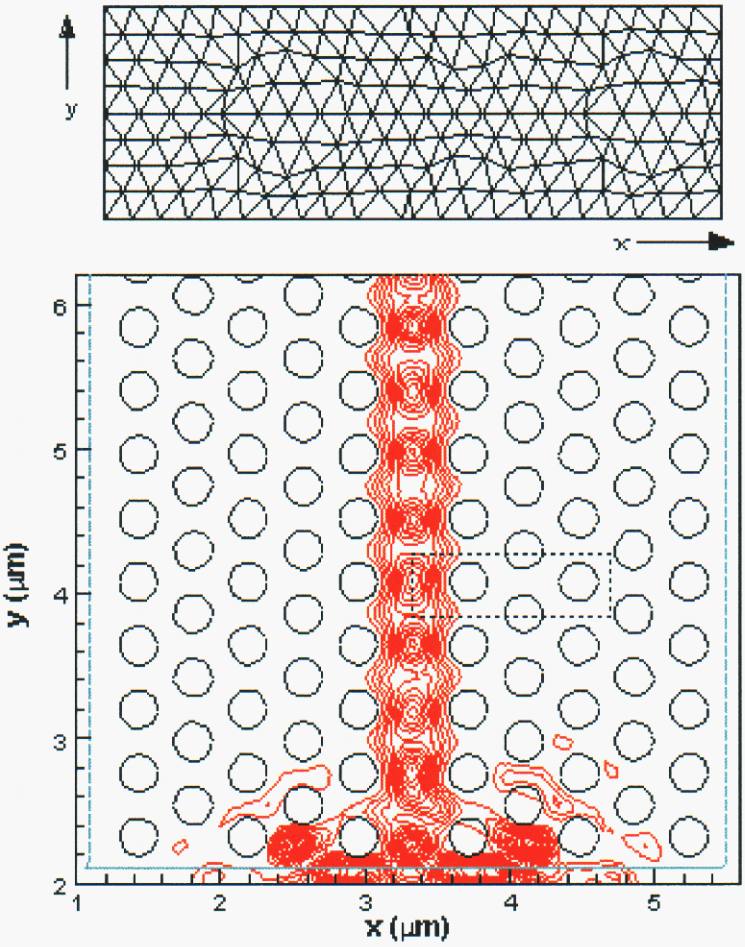

Fig. 17. (lower) Propagation of light through a row-defect waveguide in a two-dimensional photonic crystal. (upper) Meshing in lateral dimension of dotted outline in lower plot used in three-dimensional loss calculation

The other problem involved the truncation of the problem in the x direction (see *Fig. 17).* Although the results of the 2D simulations gave the impression that the inclusion of three rows of holes should be sufficient for the 3D calculations, this was found not to be the case. Although including many rows was not possible due to the rapid increase in computer memory required, calculations performed with nine rows of holes gave very

different results from previous calculations including few rows. This is illustrated in *Fig. 18,* where certain features present in the earlier three-hole calculations, such as the low-loss dips and high-loss resonance peaks, are found to disappear when a wider problem region is used, as seen from the curve for nine rows of holes. This leads to the conclusion that these features resulted from reflections from the lateral problem boundary. The later calculations also agree better with the results of Lalanne [4] (also shown in the figure), computed using a plane wave method and seven rows of holes. To further investigate this assertion, we have plotted field contours for the computed 3D mode of this same waveguide in *Fig. 19.* As is clearly seen, the highest intensity contours are indeed localized about the lower left corner, as expected. However, a long low-intensity tail is seen stretching to the right all the way to the absorber at the right (lateral) problem boundary, even with nine rows of holes. This observation corroborates the previous conclusion that reflections from this boundary have been influencing the results, and it is not clear at this point how large the problem region would have to be in this direction to avoid this problem. However, it is clearly beyond the range of present computational capabilities.

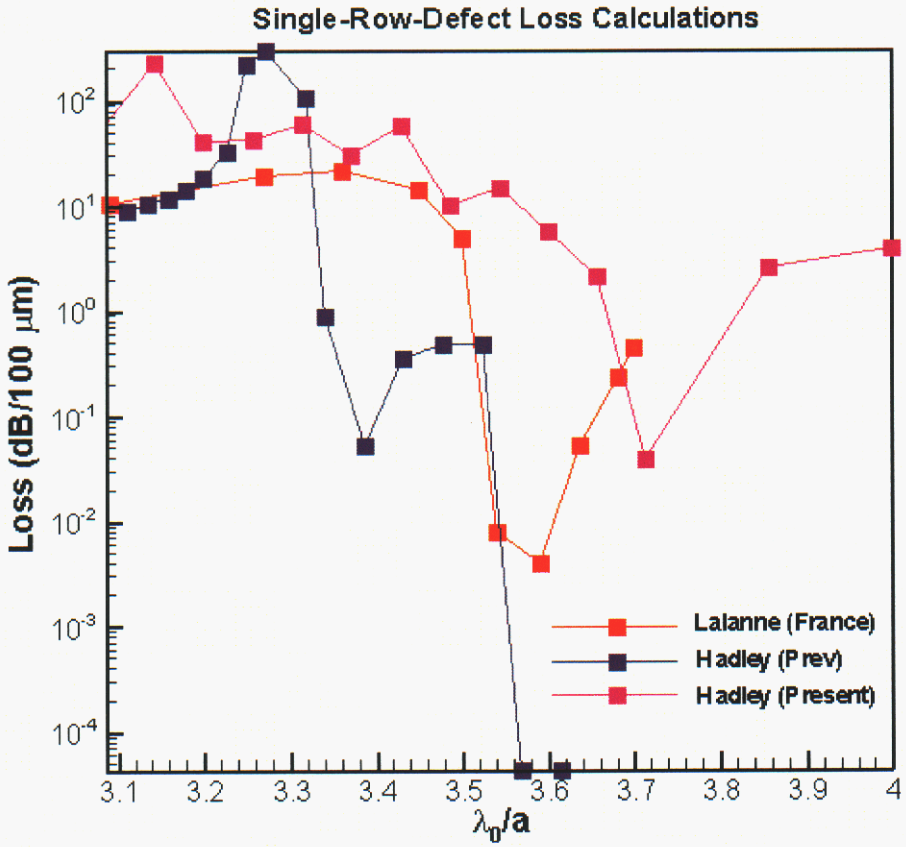

Fig. 18. Loss calculations for single-row-defect waveguide using 3 rows of holes (blue curve), 9 rows of holes (pink curve) and compared to plane wave method (red curve)

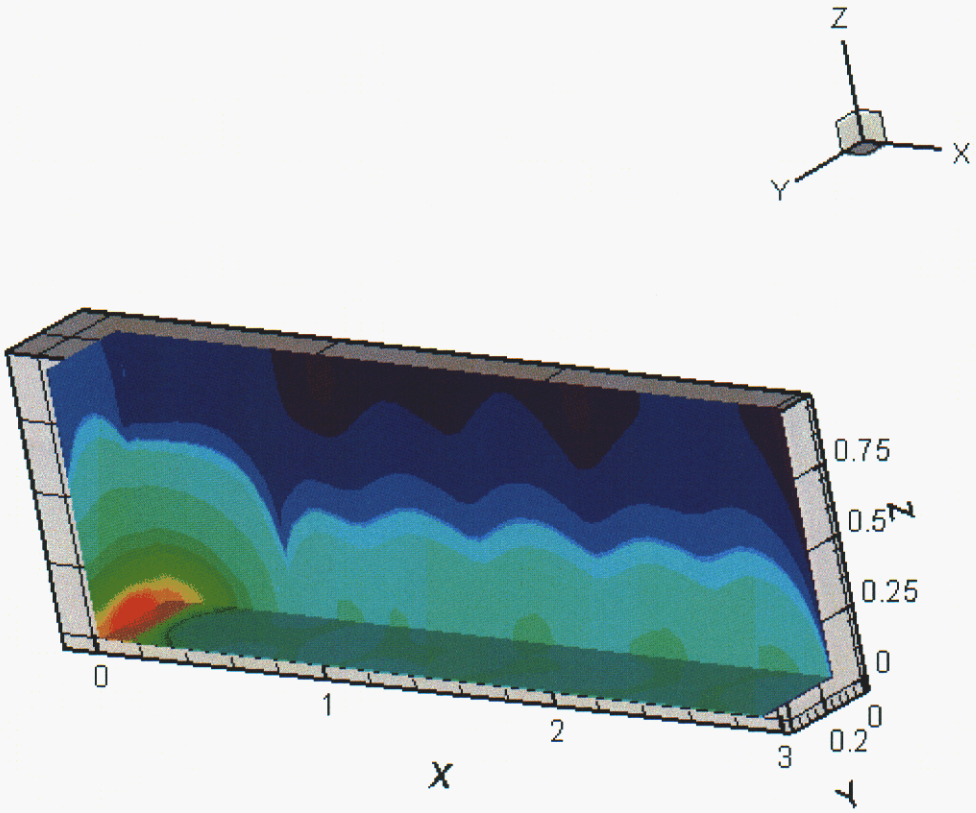

Fig. 19. Field for a row-defect waveguide mode propagating in y direction

While the problem with handling radiation is purely numerical, i.e. has no physics implications, the second problem involving the lack of lateral confinement does. It implies that single-row-defect waveguides do not confine light as completely as previously thought, and may therefore not be as attractive for waveguiding. However, it is hard to tell without further investigation what fraction of energy is contained in the "tail", making it thus impossible to quantify the above statement. Nonetheless, our investigation has clearly pointed to an issue that deserves further study.

All the curves in *Fig. 18* predict relatively large losses above the light cone, and small losses below it, as has been confirmed experimentally [5] (although for a different material system). This confirms simple theoretical concepts about the light cone, and suggests that operation below it is one method of reducing losses. Unfortunately, this restricts severely the slab geometries that may be used, and implies the use of low-index substrates which generally do not conduct current well and are thus not good candidates for integration of active devices.

Processing of the Photonic Crystal

Upon the completion of designs for photonic crystals with negative refraction characteristics (as in *Figs. 4 and 5*) and focusing characteristics (as in *Fig. 12*) experimental devices were fabricated according to the following procedure. The general cross section of the fabricated devices follows *Fig. 3(a)*. AlGaAs and GaAs epitaxial layers were deposited onto GaAs wafers using metal-organic chemical vapor deposition (MOCVD). A uniform 350 nm thick layer of SiO_2 was deposited onto the surface by plasma enhanced chemical vapor deposition (PECVD). Conventional photolithography and dry etching were then used to create launch waveguides for the refraction experiment. Localized photonic lattices were created using electron beam lithography and a spin-deposited layer of PMMA (polymethylmecacrylate) as an etch mask for the SiO_2 surface layer. The SiO_2 then served as the etch mask for the lower GaAs/AlGaAs layers. The actual photonic lattice was etched into the GaAs/AlGaAs using Cl_2 reactive ion beam etching. After final etching of the lattice the lower AlGaAs cladding was converted to a robust native oxide using steam oxidation at ~420 °C.

Fig. 20(a) is a scanning electron micrograph (SEM) of completed photonic lattice for focusing. The light comes from a singe-mode waveguide (upper left), diverges in the planar waveguide region before reaching the photonic lattice. The two-dimensional waveguide photonic lattice is designed as a focusing lens to focus the light into one of the output waveguides in the right. *Fig. 20(b)* is a detail view of the waveguide photonic lattice holes.

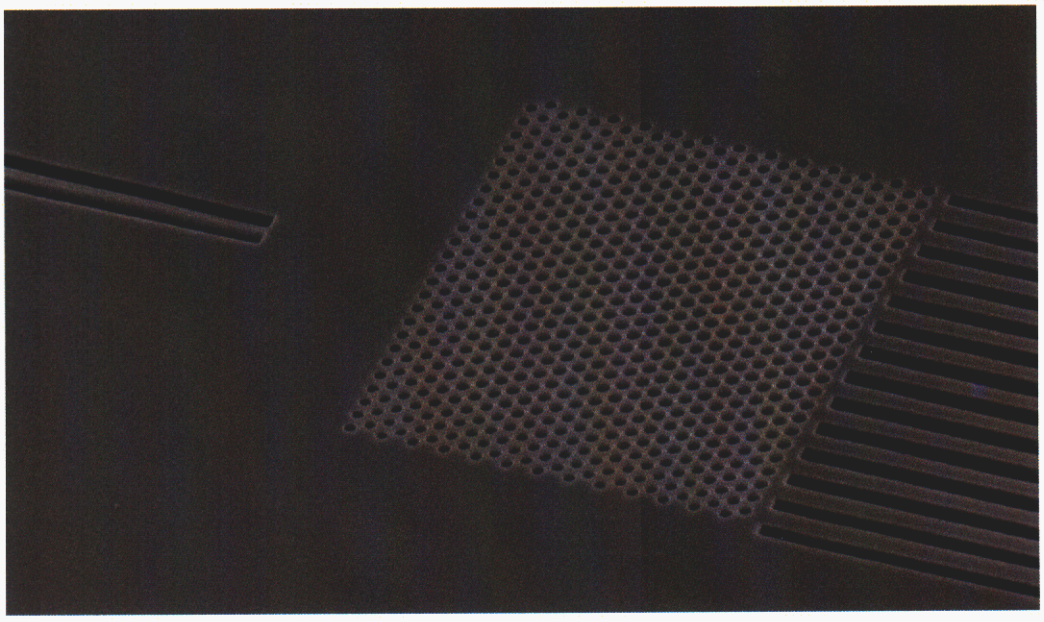

Figure 20(a). A scanning electron micrograph (SEM) of a completed waveguide photonic lattice device for focusing.

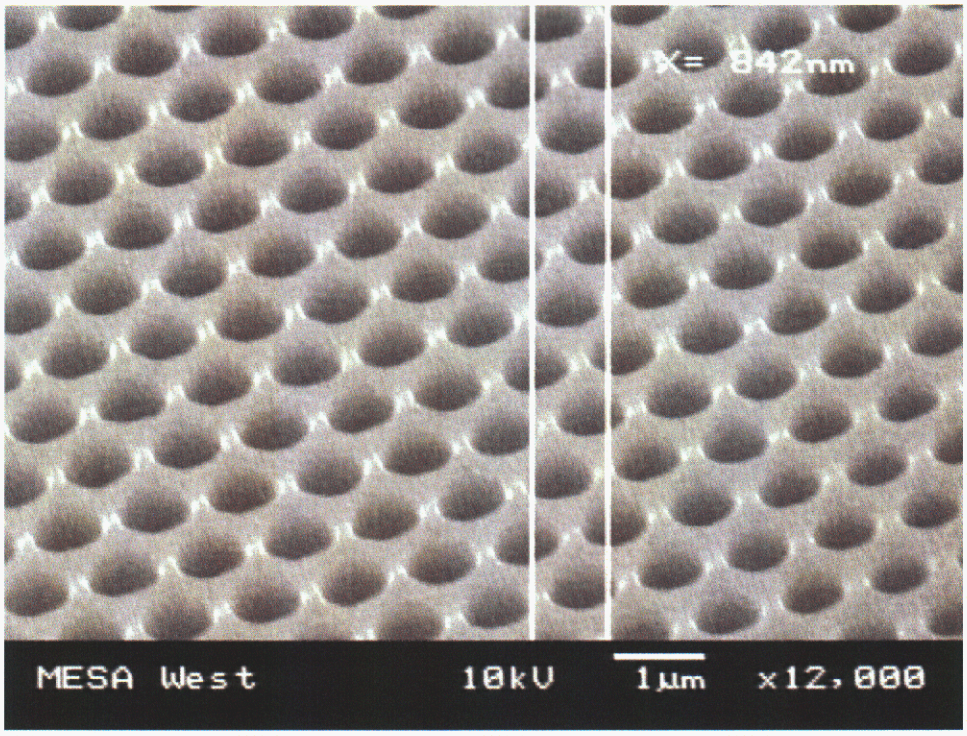

Fig. 20(b). SEM image of the waveguide PC holes.

Experimental Results

Testing of the photonic crystal devices was done by end-fire coupling a wavelength tunable (near 1550 nm) laser into the cleaved facet of the etched waveguide. The waveguides are tapered waveguides used to guide light into the desired photonic lattice devices. A high numerical aperture microscope objective lens (NA=0.85) was used to couple the light into the tapered waveguide. Light was collected after transmission through the output waveguide. Surface-normal scattered light was collected from the top of the photonic crystal using a high numerical aperture and long working distance microscope (X100, NA=0.5) and infrared imaging system. This scattered light was used to examine the propagation of light through the photonic lattice. *Fig. 21* is a photo of the test setup.

Fig. 22 is a diagram of the self-focusing photonic lattice device. Light is launched into a tapered waveguide (a deep-etched rib tapered from 5 µm to 0.25 µm in lateral dimension) that squeezes the optical mode down to the dimension needed to establish a widely divergent optical field incident onto the photonic lattice lens. The lens is then intended to focus the light onto one of output array waveguides that are to be used to measure the near field optical intensity profile at the exit side of the lattice. *Fig. 23* is an image of the light scattered out the top of the photonic crystal lens structure at the wavelength of

1545nm. A feint outline of the waveguide and lattice structure is superimposed onto the scattered light image as an aid to understanding light propagation in the photonic lattice. Considerable scattered light is observed as light exits the tapered waveguide and enters the photonic lattice. Once inside the photonic lattice a much more feint series of spots is seen to converge to a single point on the exit side of the lattice. This convergence is consistent with the desired focusing behavior. However, the scattered signal decays rapidly with propagation through the lattice in a manner suggestive of very high transmission losses. The transmission loss is apparently so high as to prevent any measurable light from reaching the far side of the lens and coupling into the array of output waveguides.

Fig. 24 shows the wavelength dependence of the optical field distribution inside the photonic lattice. As we change the wavelength (frequency), the 2-D k-vector changes in the photonic lattice region. As a complete linear electromagnetic system, the optical field distribution will change accordingly. Although the evidence is not extremely strong, we believe that the optical field has been focused within the photonic lattice lens. Figure 24 (c) particularly shows the focusing effect of the photonic lattice lens. The two bright spots (top and bottom) are associated with the k-vectors which fall off the self-focusing or self-collimating angle (see Figure 15). Since the frequency is well above the lightline of the photonic lattice for out-of-plane total internal reflection, the loss is intrinsically high.

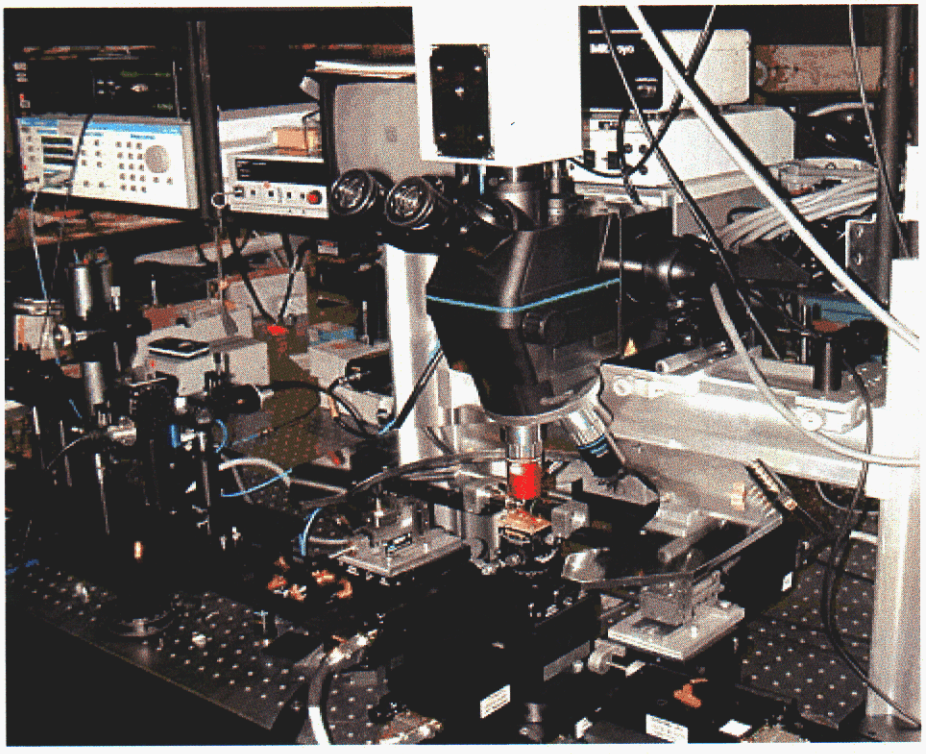

Fig. 21: The waveguide test apparatus used to evaluate photonic lattice devices.

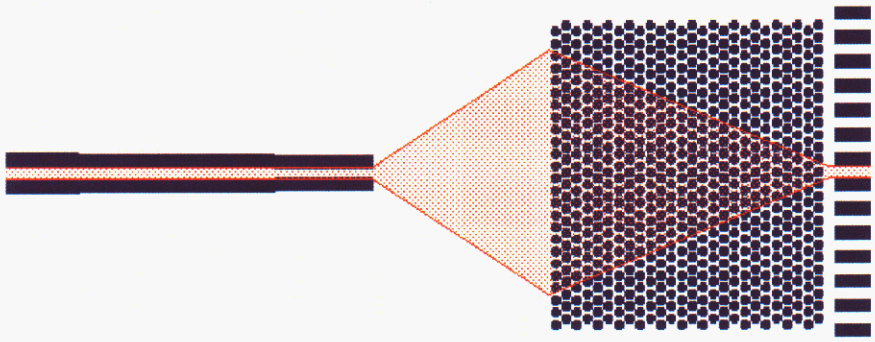

Fig. 22. Sketch of the photonic lattice lens experiment. Solid blue features are etched into the wafer, such as the lattice holes seen in Fig. 20. Red markings illustrate the intended light path from the launch waveguide on the left to the photonic lattice lens and into on of the receiving waveguides on the right.

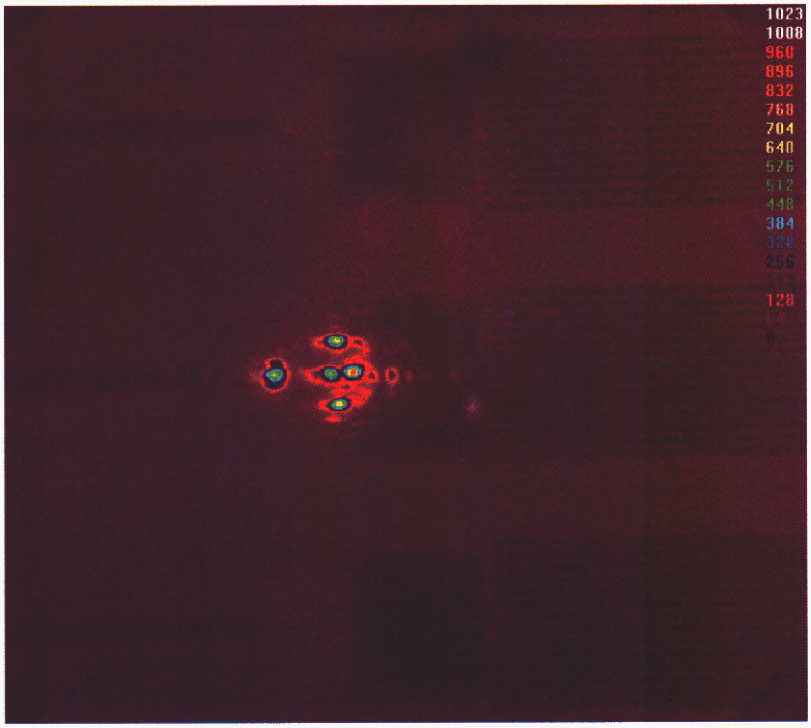

Fig. 23. False color images of light scattered out of the surface of the photonic lattice lens at 1545 nm wavelength. Refer to text and Fig. 22 for detail.

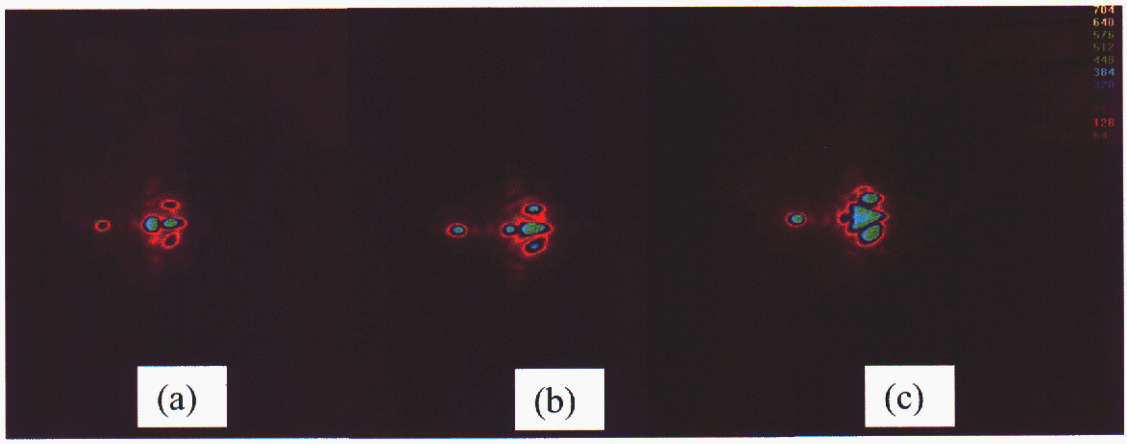

Fig. 24. Images of light scattered out of the surface of a photonic lattice lens at three different wavelengths (a) 1540 nm, (b) 1550 nm, (c) 1560 nm.

Summary

The numerical modeling of these two-dimensional row-defect waveguides led to several unexpected discoveries. The focusing effect of the negative refractive index photonic crystal is an effective coupling mechanism for row-defect waveguides. The three-dimensional modeling indicated a guided mode with a much broader guided extent than anyone expected, as first inspection seems to imply a tightly-bound mode in a row-defect waveguide. Losses out of plane in the modes above the light line were found to be quite high. Whether these losses can be managed so that the interesting properties apparent in modes above the light cone can be exploited has yet to be determined and warrants further investigation. Likewise, the collimating effect also deserves further study as it offers a waveguiding mechanism that eliminates the need for a row defect and its corresponding high losses.

Conclusions

Our investigation has shown that laterally dispersive 2D photonic lattice devices are inherently lossy due to the requirement to operate well above the light line. Though uninvestigated, losses are many dB/mm. We have evidence, though not compelling, of focusing behavior in our design but losses are too high to measure light transmission completely through the lens structure. Similarly, Krauss [6] has published limited results for refraction of a plane wave using a much shorter photonic lattice section. Other than these, the only experimental work is by Kosaka [3] using 3D autocloned photonic lattices. This 3D system employs a complex vertical layer structure serving to suppress out-of-plane radiation. However, such 3D systems are much more difficult to fabricate and exploit as planar photonic lightwave circuits, as has been the focus of this research program. Therefore a significant challenge remains to demonstrate, experimentally or numerically, a 2D laterally dispersive optic element with sufficiently strong refraction characteristics and size (i.e., low loss) that it is capable of separating wavelengths or of bending light in a useful fashion. At this point, further research must focus on reducing losses in these photonic crystals operated above the light line where the lateral dispersion effects are most interesting.

Row defect waveguides have continued to advance with recent reports of low loss, 1.5 dB/mm, in a silicon-on-insulator structure [7] and of strong group velocity dispersion [7-8] leading to slow-wave propagation. At the same time recent investigation of self-collimating light propagation in this work and else where [9] has opened the possibility that row defect waveguides may not be required. In fact, losses of self-collimated propagation have already reached 2 dB/mm [10], about the same as the best row-defect waveguides.

The implications of all these developments is that silicon-on-insulator (SOI) technology is emerging as the technology platform of choice and that optimal ultra-high-performance

planar lightwave circuit will be built of a combination of localized photonic lattice devices interconnected by conventional ridge waveguides. Si ridge waveguides have losses as low as 0.8 dB/cm and abrupt 90 degree bends with excess loss as low as 0.5 dB. With such low loss interconnection using conventional waveguides, localized photonic lattice devices are best used for uniquely enabling capabilities such as dispersion compensation, multi-pole wavelength channel add/drop, wavelength selective 1xN splitters, combiners, and routers [11]. One very interesting recent development is the proposal of an optical isolator in a 2D photonic lattice configuration [12]. If the isolation function is proven experimentally this represents a class of non-reciprocal optical devices which cannot be fabricated using conventional waveguides and that would dramatically enhance lightwave circuit functionality by controlling optical feedback interactions between circuit sections.

All of the above lightwave circuit technologies can be transferred to compound semiconductors, through the use of wafer bonding methods, to form the compound semiconductor analog to the SOI device. Fabricating these devices in compound semiconductors will enable integration with light emitters and detectors, either conventional or photonic crystal based, to round out the lightwave circuit device suite.

References

[1] D. W. Prather, J. Murakowski, S. Shi, S. Venkataraman, A. Sharkawy, C. Chen, D. Pustai, "High-efficiency coupling structure for a single-line-defect photonic-crystal waveguide," Opt. Lett., vol. 27, pp. 1601-1603, Sept. 2002.

[2] M. Notomi, "Theory of light propagation in strongly modulated photonic crystals: Refractionlike behavior in the vicinity of the photonic band gap," *Phys. Rev. B*, vol. 62, pp. 10696-10705, 15 Oct. 2000.

[3] H. Kosaka, T. Kawashima, A. Tomita, M. Notomi, T. Tamamura, T. Sato, and S. Kawakami, "Superprism phenomena in photonic crystals," Phys. Rev. B, vol. 58, pp. 10096–10099, 15 Oct. 1998.

[4] P. Lalanne, "Electromagnetic Analysis of Photonic Crystal Waveguides Operating Above the Light Cone", IEEE J. Quantum Electron. 38, pp. 800-804 (2002).

[5] M. Notomi, A. Shinya, K. Yamada, J. Takahashi, C. Takahashi, and I. Yokohama, "Singlemode transmission within photonic bandgap of width-varied single-line-defect photonic crystal waveguides on SOI substrates", *Electronics Letters*, vol. 37, no. 5, pp. 292-293, (2001)

[6] T. Krauss, L. Wu, T. Karle, "Dispersion engineering in photonic crystal waveguides," Proceedings of SPIE, Vol. 4655, pp. 48-52 (2002).

[7] M. Notomi, "Photonic band gap waveguides and resonators," LEOS 2003, IEEE LEOS Annual Meeting, TuE2, Tuscon, AZ (2003).

[8] M. Davenco, D. Blumenthal, "Exploring slow and dispersive propagation in 2D line-defect photonic crystal waveguides," LEOS 2003, IEEE LEOS Annual Meeting, TuE4, Tuscon, AZ (2003).

[9] T. Krauss, L. Wu, T. Karle, " Dispersion engineering in photonic crystal waveguides", Proceedings of SPIE, Vol. 4655, pp. 48-52 (2002).

[12] D. Chigrin, S. Enoch, C. Torres, G. Tayeb, "Self-guiding in two-dimensional photonic crystals", Proceedings of SPIE, Vol. 4655, pp. 63-72 (2002).

[13] D. W. Prather, J.A. Murakowski, S. Venkataraman, P. Yao; A. Balcha; T. Dillon, D. Pustai, "Enabling fabrication methods for photonic band gap devices," Proceedings of the SPIE - The International Society for Optical Engineering, vol. 4984, pp .89-99 (2003).

[14] A. Sharkawy, S. Shi, D. Prather, "Heterostructure photonic crystals: theory and applications," Applied Optics, 41(34), pp. 7245-7253 (2002).

[15] M. Soljacic, C. Luo, J. Joannnopoulos, "Nonlinear photonic crystal microdevices for optical integration," Optics Letters, 28(6), pp. 637-639 (2003).

Distribution:

2	MS 0603	David Peters, 01743
2	MS 0603	Ronald Hadley, 01742
2	MS 0603	Allen Vawter, 01742
2	MS 0603	Ganesh Subramania, 01743
2	MS 0603	Joel Wendt, 01743
2	MS 0603	Junpeng Guo, 01742
1	MS 0603	James Hudgens, 1743
1	MS 0603	Charles Sullivan, 1742
1	MS 9018	Central technical Files, 08945-1
2	MS 0899	Technical library, 09616
1	MS 0323	D. Chavez, LDRD Office, 1011